Int J Earth Sci (Geol Rundsch) (2003) 92:364–379
DOI 10.1007/s00531-003-0332-0

ORIGINAL PAPER

Nicola Capuzzo · Robert Handler · Franz Neubauer · Andreas Wetzel

Post-collisional rapid exhumation and erosion during continental sedimentation: the example of the late Variscan Salvan-Dorénaz basin (Western Alps)

Received: 4 February 2002 / Accepted: 28 February 2003 / Published online: 17 June 2003

Abstract The Salvan-Dorénaz intramontane basin formed between ca. 308–293 Ma as an asymmetric graben along crustal-scale transtensional fracture zones within the Aiguilles-Rouges crystalline massif (Western Alps) and represents a feature of the post-collisional evolution of the Variscan orogens. It contains 1.5–1.7 km of continental clastic deposits which were eroded from granitic, volcanic, and metamorphic rocks. Textural and compositional immaturity of the sandstones, and the numerous lithic fragments with low chemical and physical stability suggest only short-range transport. $^{40}Ar/^{39}Ar$ analyses of detrital muscovite are interpreted to represent cooling of the crystalline basement below the respective closure temperatures. Ages from detrital muscovite range between ca. 280–330 Ma. $^{40}Ar/^{39}Ar$ white mica plateau ages from granitic boulders range between 301–312 Ma and suggest rapid cooling. The very short time interval recorded between the $^{40}Ar/^{39}Ar$ cooling ages and the stratigraphic age of the host sediment suggests that considerable portions of the upper crust were removed prior to the formation of the basin. Late Variscan granitic boulders document surface exposure and erosion of Late Carboniferous granites during early stages of the infilling of the basin. Therefore, unroofing of basement units, magmatic activity, and formation of the fault bounded Salvan-Dorénaz basin were acting concomitantly, and are highly suggestive of extensional tectonics. When compared with other orogens, this situation seems specific to the Variscan, especially the exclusively young ages of detrital material, however, modern analogous may exist.

N. Capuzzo · A. Wetzel (✉)
Geologisch-Paläontologisches Institut,
Universität Basel,
Bernoullistrasse 32, 4056 Basel, Switzerland
e-mail: Andreas.Wetzel@unibas.ch

R. Handler · F. Neubauer
Institut für Geologie und Paläontologie,
Universität Salzburg,
Hellbrunnerstrasse 34/III, 5020 Salzburg, Austria

Keywords Exhumation · Sediment provenance · Ar-40/Ar-39 chronometry · Mica · Late Paleozoic · Western Alps

Electronic Supplementary Material Supplementary material is available for this article if you access the article at http://dx.doi.org/10.1007/s00531-003-0332-0. A link in the frame on the left on that page takes you directly to the supplementary material.

Introduction

The Variscan orogeny resulted from a collision of Gondwana and Gondwana-derived microplates with the southern margin of Laurasia, accomplished by progressive closure of the Proto-Tethys and the Iapetus oceans (Franke 1989; Ziegler 1989, 1990; Stampfli 1996; Tait et al. 1997; Stampfli et al. 1998; Neubauer and Handler 2000; Ziegler and Stampfli 2001). In western Europe, Variscan collisional tectonics commenced in the early Devonian resulting in crustal thickening and regional metamorphism, and lasted until the late Carboniferous (e.g., Franke 1992, and references therein). By this period, its evolution was characterised by concomitant rapid exhumation of medium- and high-grade metamorphic core complexes (von Raumer 1998; Zeh et al. 2000, and references therein), intense intrusive and extrusive magmatic activity (Bonin et al. 1993; Schaltegger 1997; Cortesogno et al. 1998; Capuzzo and Bussy 2000), and rapid subsidence within an array of mainly continental basins which formed discontinuously during the Late Carboniferous and Early Permian along extensional and transtensional crustal-scale fractures (e.g., Franks 1968; Cassinis and Neri 1990; Schaltegger and Corfu 1995; Stollhofen and Stanistreet 1994; Schäfer and Korsch 1998; Capuzzo and Wetzel 2003). The post-collisional evolution of the western European Variscan orogen has been compared as an analogue to the present-day Tibetan Plateau and to the Basin and Range Province (e.g., Ménard and Molnar 1988). In contrast, Ziegler (1990,

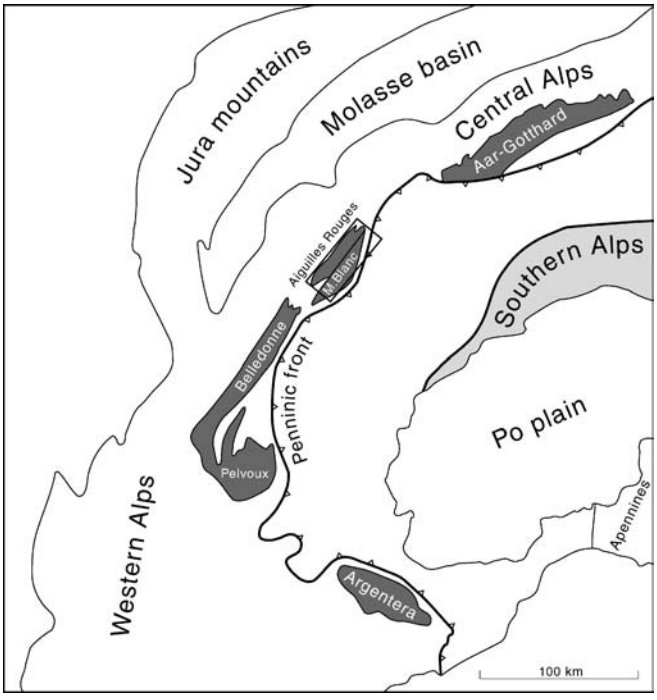

Fig. 1 Pre-Mesozoic basement rocks in the Alps (*shaded*) and External Alpine Crystalline Massifs (*dark shaded*; modified after Schaltegger and Corfu 1995). The location of the study area is *framed*

1993) suggested that the post-convergent destruction of the Variscides was caused primarily not by body-forces but by far-field stresses initiated by the dextral motion of Gondwana relative to Laurasia, which progressively propagated from the internal part of the orogen to its foreland (e.g., Arthaud and Matte 1977). Therefore, the Late Carboniferous evolution of the European Variscan orogen provides an excellent case to investigate the disruption of an orogenic belt by late orogenic, post-collisional processes.

Clastic sediments filling intra- and perimontane Permo-Carboniferous basins record the tectono-metamorphic and magmatic history at the end of the convergence (Henk 1999). Such basins are suitable for establishing the general tectonic setting as their texture and composition are primarily linked to the source-area geology, depositional environment and climate (e.g., Dickinson 1974; Bhatia and Crook 1986; Ingersoll 1988). Single detrital grains, in addition, can document the nature and of the evolution of the sediment source area, including information about its age and cooling history, especially when compared to the age of the host sediments (e.g., Copeland and Harrison 1990; Harrison et al. 1993).

It is the purpose of this paper to investigate the Late Paleozoic post-collisional history of an internal sector of the Variscan orogenic belt by studying the nature and origin of Upper Carboniferous sediments outcropping in the Salvan-Dorénaz basin (Western Alps). In order to decipher the amount of tectonic movement the chronometric ages of detrital muscovites from clastic sediments and boulders sampled at different stratigraphic levels were related to the stratigraphic age of the host sediment. In combination with petrographical and geochemical data for boulders and sediments, the $^{40}Ar/^{39}Ar$ muscovite chronometric ages constrain the geology of the sediment source area, document the history of the metamorphic/magmatic basement units just before erosion, and provide additional information on their exhumation. All these data, when compared to those from other Late Paleozoic basins of the European Variscan belt, provide new evidence about tectonic and erosional processes acting in an orogenic mountain belt.

Geological setting

The Salvan-Dorénaz basin is surrounded by the Aiguilles-Rouges metamorphic and crystalline massif that belongs to the Crystalline External massifs of the Alps (Fig. 1). These massifs represent the southern part of the former Moldanubian internal domain of the western European Variscan belt (von Raumer 1998 and reference therein). The Aiguilles-Rouges massif consists of basement nappes or slices that form Alpine antiform cores mantled by Mesozoic cover successions. They consist of a complex of granitic intrusions and polymetamorphic, amphibolite facies-grade rocks which are crossed by major, steeply dipping, N-S to NNE-SSW trending faults and mylonitic zones (von Raumer et al. 1999). In the Aiguilles-Rouges massif, an early record of the Variscan collision is represented by the decompression of a few eclogite-grade units (14 kbar, min. 700 °C; Schulz and von Raumer 1993). Widespread paragneisses experienced several deformation events related to early thrust tectonics and nappe stacking with development of a Barrovian-type metamorphism; these units display cooling ages between 337–316 Ma (Dobmeier 1998; von Raumer 1998; Bussy et al. 2000; Fig. 2). Subsequent isothermal decompression was reported from kyanite and sillimanite-bearing micaschist and gneiss, and has been interpreted as a late stage of rapid tectonic uplift during cooling (Schulz and von Raumer 1993). In addition, contrasting metamorphic P–T paths that occur over short distances have been related to "telescoping" along steeply dipping, strike-slip zones (Schulz and von Raumer 1993).

The Variscan magmatic activity in the Aiguilles-Rouges massif consisted of short-lived pulses (e.g., Bonin et al. 1993; Bussy and Hernandez 1997). Early Carboniferous syntectonic intrusions occurred at 330 Ma along major transpressive faults (e.g., Pormenaz monzonite, Bussy et al. 1997; Montées-Pélissiers peraluminous granite, Bussy et al. 2000; Fig. 2). Subsequent magmatic activity at shallow crustal levels is documented by the syntectonic intrusions of the Vallorcine and the Montenvers anatectic granites (Brändlein et al. 1994; Morard 1998). They were emplaced at 307 Ma along dextral transtensional shear-zones (Bussy et al. 2000; U/Pb-dated zircons and monazites; Fig. 2). In addition, several subvolcanic dykes crosscut the basement units (Brändlein

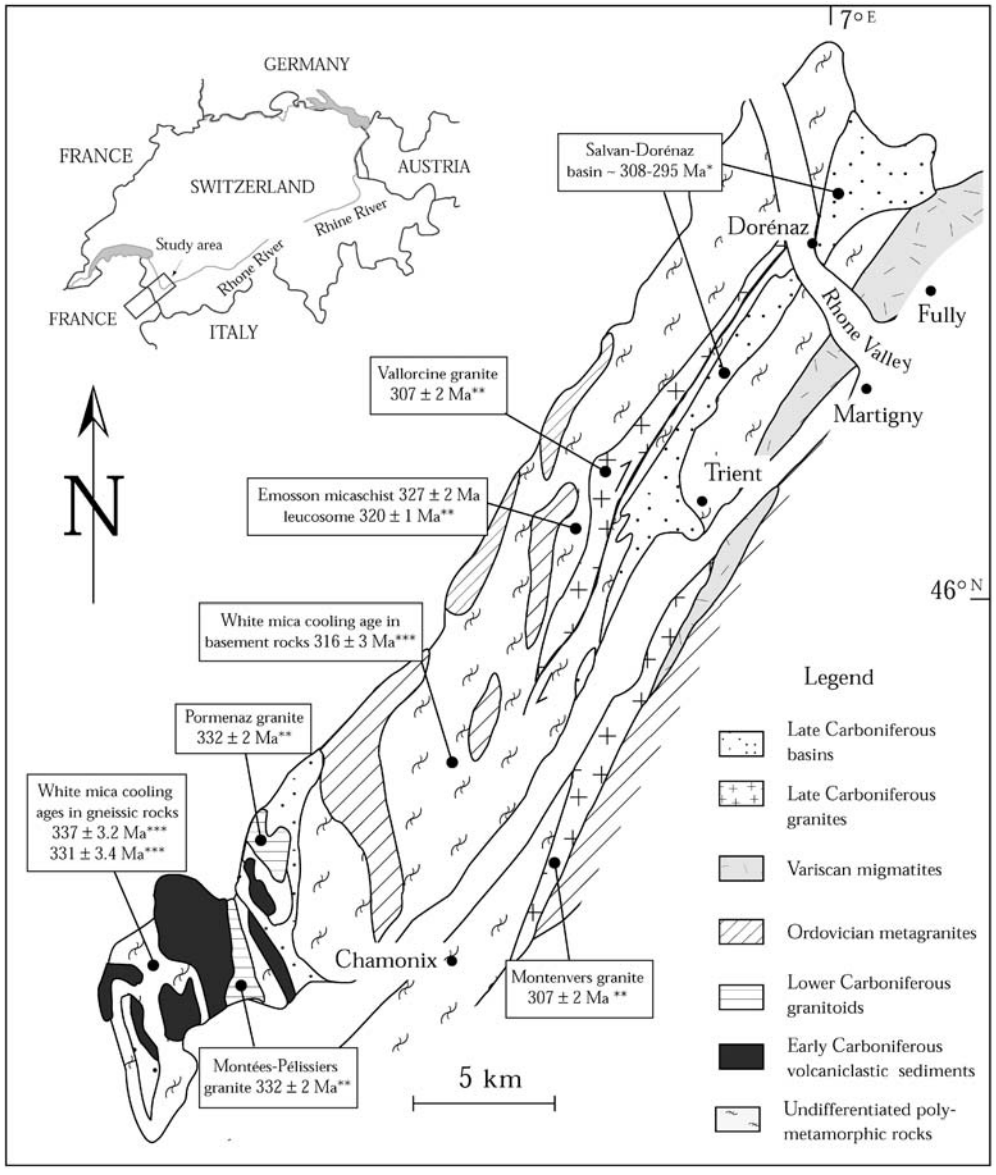

Fig. 2 Location (*upper left insert*), and geological map of the Aiguilles-Rouges massif (modified after Brändlein et al. 1994). The Late Carboniferous Salvan-Dorénaz basin follows the northeastern margin of the massif. Isotopic ages of basement and Late Carboniferous volcanic deposits are in text frames. Isotopic ages: *** $^{40}Ar/^{39}Ar$ on muscovite (Dobmeier 1998); ** U/Pb on zircon and monazite (Bussy et al. 2000); * U/Pb on zircon (Capuzzo and Bussy 2000)

et al. 1994). Subaerial lava domes and possibly ignimbritic flows have been related to subvolcanic and volcanic activities during the intrusion of the Vallorcine granite (Capuzzo and Bussy 2000).

During the Late Carboniferous in the study area, the fault bounded intramontane basins of Pormenaz and Salvan-Dorénaz formed (Sublet 1962; Lox and Bellière 1993; Dobmeier and von Raumer 1995; Niklaus and Wetzel 1996; Capuzzo and Wetzel 2003). The latter developed as an elongated asymmetric graben today exposed for about 25 km in a NNE–SSW direction along the eastern margin of the Aiguilles-Rouges massif (Capuzzo and Wetzel 2003; Fig. 2). The Salvan-Dorénaz basin crops out in a complicated syncline structure formed during Alpine deformation (Pilloud 1991; Badertscher and Burkhard 1998; Fig. 3). It contains about 1.5–1.7 km of clastic continental sediments mainly derived from erosion of metamorphic, crystalline and volcanic source area (Sublet 1962, Niklaus and Wetzel 1996). These Late Carboniferous sediments record only low metamorphic grade (upper anchizone) Alpine events, with temperatures <300 °C estimated from illite crystallinity analyses on mudstones and from vitrinite reflectivity on coals (Kubler et al. 1979; von Raumer 1971; Pilloud 1991; Frey et al. 1999). Therefore, detrital minerals as muscovite should preserve the isotopic signature of the Variscan events (see below). The Late Paleozoic deposits are truncated by a low angular unconformity overlain by shallow-marine Triassic sediments (Demathieu and Weidmann 1982; Pilloud 1991).

The Salvan-Dorénaz deposits were subdivided into four informal depositional units (Niklaus and Wetzel 1996; Capuzzo and Wetzel 2003; Fig. 3). A lower, mainly conglomeratic, alluvial fan system derived from western source areas (Unit I), overlain by fine-grained anastomosed rivers and muddy floodplain deposits (Unit II),

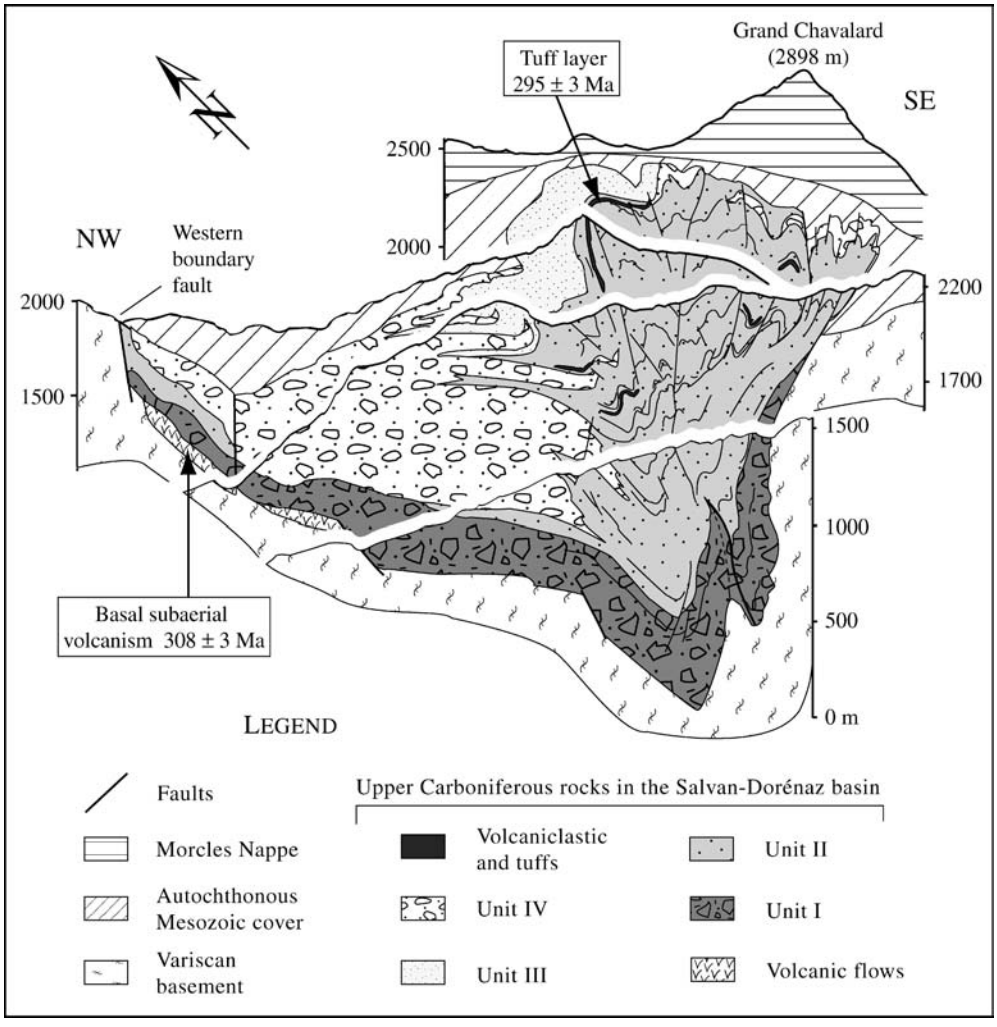

Fig. 3 Schematic cross sections representing the northeastern areas of the Salvan-Dorénaz basin (modified after Pilloud 1991). The basin fill is subdivided into four informal lithostratigraphical units (Niklaus and Wetzel 1996). Alpine deformation produced the Salvan-Dorénaz complex syncline structure. Isotopic ages of volcanic deposits after Capuzzo and Bussy (2000)

which are replaced by sand-rich meandering river deposits (Unit III). In addition, an alluvial fan system (Unit IV) several times prograded onto and retreated from the basin floor deposits of Unit II and III. A tectonic control of such cycles has been invoked, for instance, by Blair and Bilodeau (1988).

The time of formation and filling of the basin was first obtained from macroflora determination, suggesting Westphalian to Stephanian ages (Jongmans 1960; Weil 1999). U/Pb isotopic age determinations on zircons from basal volcanic deposits and from tuff layers at different stratigraphic levels of the basin indicate a minimum age for basin formation at 308±3 Ma (Capuzzo and Bussy 2000). On the other hand, a tuff layer outcropping ca. 200 m below the unconformity to the Triassic deposits produced a concordant age of 295±3 Ma (Capuzzo and Bussy 2000; Fig. 3). From the average subsidence rate calculated during the development of the basin (>0.1 mm/year) an upper time limit at 293 Ma can be assumed for the preserved clastic record in the Salvan-Dorénaz basin.

Samples and analytical methods

To evaluate the geology within the basin-fill source areas, sediments and their constituents were analysed petrographically and geochemically. In addition, $^{40}Ar/^{39}Ar$ geochronology on muscovites was carried out to elucidate the processes within the catchment areas.

Whole rock major and trace element concentrations were measured on pressed and glass pills by X-ray fluorescence spectrometry (XRF; Philips PW 1400 equipment) at the Centre d'Analyse Minérale of the University of Lausanne (Switzerland). Data are reported in Table 1.

Six samples of individual granitic and gneissic boulders, 8–120 cm in diameter, were selected from the lowermost Unit I for whole-rock major and trace elements geochemistry and for bulk-grain step-heating $^{40}Ar/^{39}Ar$ geochronology on muscovite (Table 2).

Eight sediment samples containing abundant detrital white mica were selected for $^{40}Ar/^{39}Ar$ geochronology on muscovite. About 1–2 kg of fresh and well-cemented conglomerates and sandstones were collected at different stratigraphic levels of the Salvan-Dorénaz basin (Fig. 4). Short descriptions of sampling locations are reported in

Table 1 Chemical composition of the major and trace elements for the analysed samples. See text for description and Table 2 for location of samples

	Gneiss boulder CN239	Granitic boulder CN337	Pegmatitic boulder CN338/a	Granitic boulder CN338/b	Granitic boulder CN340	Vallorcine granite FB1030	Vallorcine granite CN331
Major elements							
SiO_2	74.70	72.63	72.42	74.36	75.27	71.33	73.50
TiO_2	0.07	0.15	0.04	0.03	0.03	0.29	0.08
Al_2O_3	14.49	14.59	14.38	13.25	12.85	15.19	14.42
Fe_2O_3[a]	0.48	1.43	0.62	0.92	0.40	1.92	0.51
MnO	0.02	0.06	0.07	0.05	0.06	0.03	0.01
MgO	0.20	0.62	0.38	0.37	0.21	0.62	0.16
CaO	1.51	1.86	2.89	2.39	2.71	0.64	0.37
Na_2O	4.81	3.88	2.76	4.00	4.87	3.22	3.11
K_2O	1.91	2.25	2.82	1.51	1.21	5.24	7.41
P_2O_5	0.28	0.21	0.16	0.02	0.02	0.34	0.12
Cr_2O_3	0.00	0.00	0.00	0.00	0.00	0.00	0.00
LOI	1.61	2.42	3.08	2.13	2.22	1.04	0.28
Total	100.07	100.12	99.62	99.02	99.84	99.86	99.97
CIA	0.55	0.55	0.54	0.51	0.48	0.57	0.52
A/CNK	1.14	1.19	1.12	1.06	0.90	1.25	1.04
Trace elements							
Nb	14	17	14	19	20	19	7
Zr	15	71	20	61	64	117	25
Y	7	10	9	35	41	6	11
Sr	182	141	158	111	116	90	155
U	<2<	6	4	<2<	<2<	4	<2<
Rb	89	120	134	73	58	322	256
Th	2	7	4	15	11	17	6
Pb	27	32	60	24	23	23	54
Ga	17	19	17	21	22	26	16
Zn	17	26	18	52	18	55	26
Cu	11	7	10	10	7	10	11
Ni	<2<	3	<2<	<2<	<2<	3	3
Co	25	36	28	38	44	43	26
Cr	9	11	11	6	5	10	11
V	4	13	6	5	4	20	5
Ce	<3<	16	<3<	30	34	58	18
Nd	<4<	8	<4<	16	17	31	10
Ba	277	418	452	302	260	436	840
La	<4<	10	5	14	14	30	<4<
S	<3<	669	194	563	91	<3<	80
Hf	24	19	8	19	24	5	<1<
Sc	6	7	8	8	8	4	<2<
As	4	<3<	4	9	5	4	<3<

[a] Fe_2O_3 as total Fe

Table 2. Two samples (CN 145 and CN 146) were analysed by the conventional multiple-grain, step-heating $^{40}Ar/^{39}Ar$ geochronology (Lausanne laboratory), while the other six were investigated by single-grain total-fusion, and partly by bulk-grain incremental-heating $^{40}Ar/^{39}Ar$ analyses (Salzburg Argonautes laboratory).

Generally, the muscovite $^{40}Ar/^{39}Ar$ isotopic clock records the time of cooling through a blocking temperature of ca. 375±50 °C (Steiger and Jäger 1977; Reuter and Dallmeyer 1989; Rollinson 1993; McDougall and Harrison 1999 and references therein). Very small grains (<100 μm), however, can be of secondary origin and may provide misleading results (for details see, e.g., Frank and Stettler 1979; Reuter and Dallmeyer 1989; Simon 1990; Dallmeyer and Takasu 1992). In order to minimize the risk of dating secondary muscovites only grains >0.25 mm were measured for $^{40}Ar/^{39}Ar$ age determinations. Ages and errors were calculated following suggestions by McDougall and Harrison (1999) and decay constants reported by Steiger and Jäger (1977). For detailed analytical procedure see Appendix.

Results

Sediment petrography

The investigated sediments range from fine sandstones to conglomerates. They are classified according to Pettijohn et al. (1987) as lithic to arkosic arenites and lithic to feldspathic greywackes being of low compositional maturity.

In thin section, sandstones display clast- to matrix-supported fabrics with angular to subrounded grains. Detrital grains are principally composed of monocrystalline and polycrystalline quartz, feldspar, mica flakes,

Table 2 Location of the investigated samples. The approximate stratigraphic position in the Salvan-Dorénaz basin is shown in Fig. 4. For comparison, two additional samples from the Vallorcine granite were sampled (see text for details)

Samples	Description	Coordinates[a]
Sediments		
CN 214	Sandstone (Unit I).	564200/102500
CN 209	Conglomerate (Unit I).	563700/101900
CN 164	Sandstone (Unit I).	569625/110375
CN 145[b]	Sandstone (Unit I).	570250/110625
CN 146[b]	Conglomerate (Unit II).	570475/114175
CN 116	Sandstone (Unit II)	114295/573222
CN 131	Sandstone (Unit III).	114100/572585
CN 136	Sandstone (Unit III).	114106/572650
Boulders		
CN 239	Gneissic boulder	562300/099175
CN 252/a	Granitic boulder	564438/101100
CN 337	Granitic boulder	562725/100688
CN 338/a	Pegmatitic boulder	562725/100688
CN 338/b	Granitic boulder	562725/100688
CN 340	Granitic boulder	562725/100688
FB 1030	Vallorcine granite	561275/101975
CN 331	Vallorcine granite	568175/110950

[a] Coordinates refer to 1:25.000 Swiss National topographic maps
[b] Detrital muscovite analysed by $^{40}Ar/^{39}Ar$ multiple-grain, step-heating technique

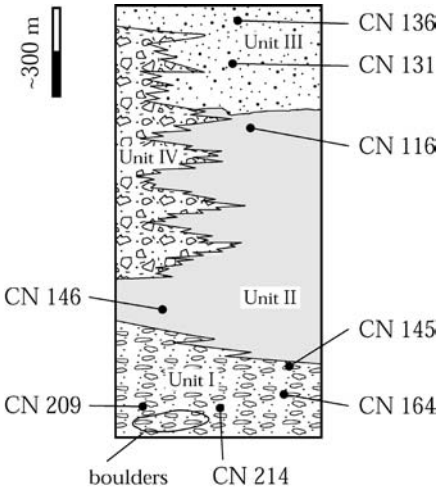

Fig. 4 Schematic section of the Late Carboniferous sediments in the Salvan-Dorénaz basin with position of the analysed samples. Lithostratigraphical units as in Fig. 3. Details of investigated samples can be found in Table 2

and lithic fragments, which are more abundant in the coarser grain sizes. Monocrystalline quartz has irregular embayments typical for volcanic quartz or undulose extinction, more characteristic for plutonic origin. Metamorphic quartz is formed by two to three irregular crystals or by several oriented crystals presenting sutured contacts. In addition, cryptocrystalline volcanic chert is present. Feldspars commonly show evidence of chemical weathering. K-feldspars are more frequent than plagioclases, which usually are fresher and probably of volcanic origin. Micas occur as large detrital flakes with elongated shapes, sometimes concentrated along laminae, and consist of varying proportions of white mica and biotite. Muscovite is normally more frequent than biotite. In few samples, high concentration of fresh detrital biotite seems to indicate distinct volcanic/magmatic sources. Lithic fragments are numerous and are mainly composed of plutonic/gneissic, biotite and muscovite micaschist and acidic volcanic fragments, denoting provenance from magmatic and metamorphic sources (Figs. 5A, B).

Boulder petrography

In thin section, the investigated magmatic boulders exhibit an equigranular to porphyritic texture and coarse (0.5–2.0 cm) to pegmatitic (>2.0 cm) grain size. Among the principal mineral phases are anhedral quartz and large subhedral feldspars, intensely weathered and partially or completely replaced by clay minerals (Figs. 5C–E). Large plagioclases with characteristic albite twinning are sometimes selectively altered (Fig. 5C). K-feldspar may show poikilitic texture (Fig. 5D) and is more intensely weathered (Fig. 5E). Fresh and subhedral muscovite occurs as a magmatic phase (Fig. 5C). Subordinately, a different generation of fine-grained white mica occurs within large and weathered K-feldspars. These grains might have formed dring hydrothermal alteration (e.g., Simon 1990). In specific boulders, a varying proportion of subhedral biotite flakes occurs. They are partially or completely altered into chlorite and in a few cases replaced by muscovite, as commonly noted during low-temperature hydrothermal alteration (Simon 1990). Since no signs of intense deformation and recrystallization were noticed, the emplacement of these granites is interpreted to have followed the main Variscan metamorphism. For a detailed description of the petrographical and mineralogical features of the different facies of the Vallorcine granite the reader is referred to Brändlein (1991) and Brändlein et al. (1994).

Geochemistry of boulders

Considering the depositional environment of the boulders, whole-rock chemical modification due to weathering and diagenesis can be significant (Nesbitt and Young 1989). The amount of chemical weathering in granitic rocks is strongly dependent on the climatic regime and, for example, minimum under cold and arid climates and maximum under hot and humid conditions (Nesbitt and Young 1982, 1989). Since feldspars are among the most abundant minerals of the upper crust their chemical alteration is indicative of the intensity of chemical weathering (Nesbitt et al. 1997). The intensity of chemical weathering can be measured by calculating the relative proportions between the concentrations of Al_2O_3, CaO, Na_2O and K_2O (CIA, **C**hemical **I**ndex of **A**lteration; Nesbitt and Young 1982). The analysed boulders have

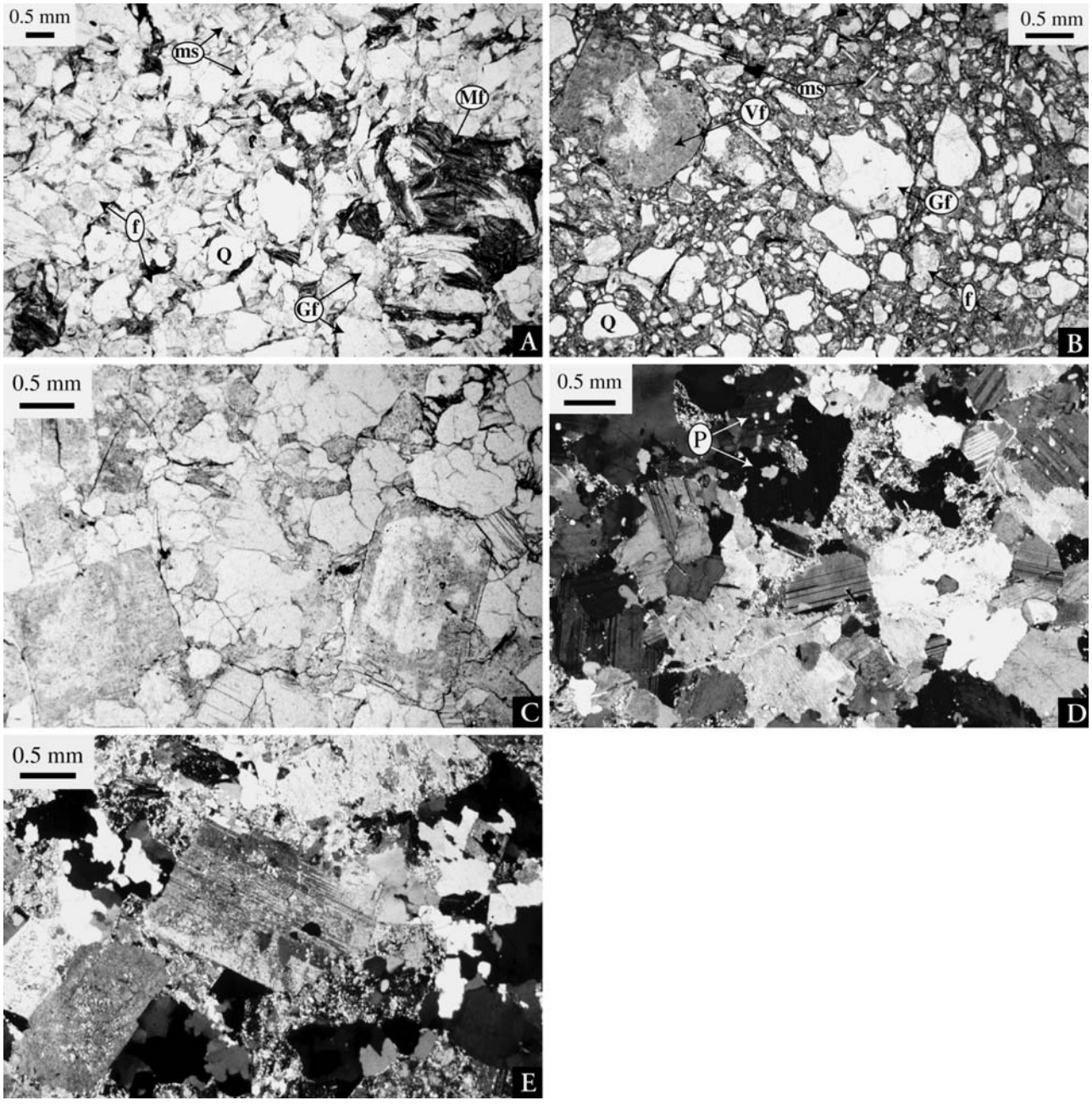

Fig. 5 **A** Clast-supported, texturally and compositionally immature lithic arenite (sample CN 214), plane-polarized light; for details see text. **B** Matrix-supported, texturally and compositionally immature greywacke (sample CN 116), plane-polarized light; for details see text. **C** Medium grain size, porphyritic texture of a granitic boulder from the lower alluvial fan Unit I (sample CN 252/a), plane polarized light; feldspars are zoned and show selective alteration, muscovite occurs as a magmatic phase, no signs of post-emplacement deformations are visible; for further details see text. **D** Medium grain size, porphyritic texture of a granitic boulder from the lower alluvial fan Unit I (sample CN 340) in cross-polarized light; feldspars present characteristic albite twinning and may show poikilitic texture with quartz (*P*); no signs of post-emplacement deformations are visible; for details see text. **E** Medium grain size, granitic boulder from the lower alluvial fan Unit I (sample CN 337) under cross-polarized light; porphyritic feldspars have subhedral shapes and show alteration in clay minerals and secondary fine-grained muscovites; no signs of post-emplacement deformations are visible. *Gf* Gneissic and/or granitic fragments; *Mf* micaschists fragments; *Vf* volcanic fragments; *Q* quartz; *f* feldspars; *ms* detrital muscovite flakes

CIA values between 0.48 and 0.55 (Fig. 6, Table 1), which are in the range of fresh granites (0.45–0.55; Visser and Young 1990). These values are very similar to those determined for the Vallorcine granite (0.52–0.57; Fig. 6, Table 1); the samples from the Vallorine granite, however, present slightly lower SiO_2, higher total alkali (8.5%–10.5%), and similar Al_2O_3 concentrations (Table 1). In addition, CaO is higher in the boulders, whereas

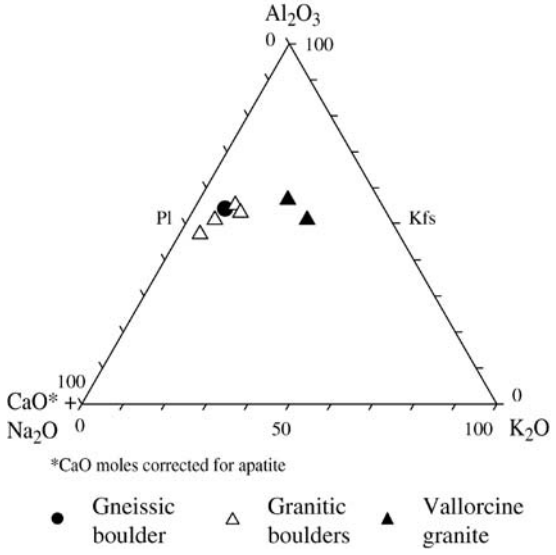

Fig. 6 Chemical indexes of alteration (CIA) after Nesbitt and Young (1984, 1989) show only moderate chemical weathering (low CIA), and limited alteration of the major elements. Whole-rock chemical data are reported in Table 1, samples in Table 2. CIA=$Al_2O_3/(Al_2O_3+CaO^*+Na_2O+K_2O)$; all oxides are in mol%; CaO* considers only CaO associated with silicate minerals (Nesbitt and Young 1984)

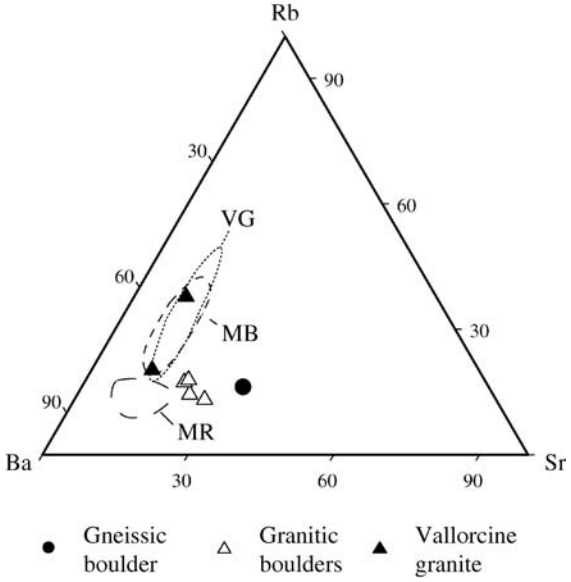

Fig. 7 Trace element discrimination diagram for granitic rocks based on relative proportions of Sr, Rb and Ba (after El Bouseily and El Sokkary 1975). Fields for Vallorcine granite (*VG*), Mont-Blanc granite (*MB*), and Mont-Blanc rhyolites (*MR*) are after Bonin et al. (1993). Data are reported in Table 1

K_2O is much higher in samples from the Vallorcine granite (Fig. 6, Table 1), but it was not possible to determine if these chemical differences are of primary or secondary origin.

The whole rock trace elements concentrations of the boulders present similar Sr, Pb, Zn and Cu values for the Vallorcine granite, whereas Ba and Rb concentrations are significantly lower in the boulders (Table 1). This is well visualised in the discrimination diagram of El Bouseily and El Sokkary (1975), where the granitic boulders occupy a distinct field, closer to the Rb vertex, from the Vallorcine granite (Fig. 7). Leaching of K, Rb and Ba, mainly form weathering of feldspars and mobilisation of Rb during high temperature chloritization of biotite can occur during hydrothermal alteration and/or during chemical weathering (Nesbitt and Young 1984, Simon 1990).

$^{40}Ar/^{39}Ar$ white mica ages of boulders and Vallorcine granite

The muscovite bulk-grain samples from one metamorphic and five magmatic boulders were analysed by $^{40}Ar/^{39}Ar$ step-heating technique (Fig. 8, Table 2, data available as additional material "Data 1", see http://dx.doi.org/10.1007/s00531-003-0332-0). Minor loss of radiogenic Ar is indicated by younger ages reported in low-temperature gas release steps of the coarse grained (>1 mm) muscovite sample CN 239, and from the bulk-grain muscovite samples CN 337, CN 338/a, CN 338/b, as well as from the muscovite sample (FB 1030) of the Vallorcine granite (Fig. 8). Medium- and high-temperature release steps record plateaux ranging from 312.7±2.9 (sample CN 252/a) to 301.4±3.3 Ma (sample CN 340; Figs. 8a–e). $^{40}Ar/^{39}Ar$ incremental heating of a coarse-grained (>1 mm) muscovite single-grain from one gneiss boulder (CN 239; Fig. 8g) yields a more disturbed Ar-release pattern than the smaller size fraction 0.25–0.71 mm of the same boulder because of slightly older ages (Fig. 8h). The former yields a more concordant release pattern with a well defined age for the Vallorcine granite of 306.5±3.4 Ma integrated over 82.9% of the total ^{39}Ar released.

Additionally, a well-defined, concordant apparent age of 307.6±3.3 Ma (sample FB 1030; Fig. 8f) was determined for a bulk-grain sample of magmatic muscovite from upper levels of the Vallorcine granite. Within the analytical error, this $^{40}Ar/^{39}Ar$ age is similar to U/Pb zircon and monazite ages (Bussy et al. 2000; Fig. 2). All apparent $^{40}Ar/^{39}Ar$ ages are interpreted to record cooling of granite/gneiss samples through respective closure temperature of the Ar isotopic system. The low-temperature argon loss—we estimated it as ca. 1%—led to younger, post-depositional ages (for discussion see below).

$^{40}Ar/^{39}Ar$ ages of detrital white mica

In a first test, the age of the detrital muscovites (>0.25 mm) was determined by incremental-heating of seven bulk-grain samples from sandstones. Only two of them (CN 145, CN 146) showed an internally concordant

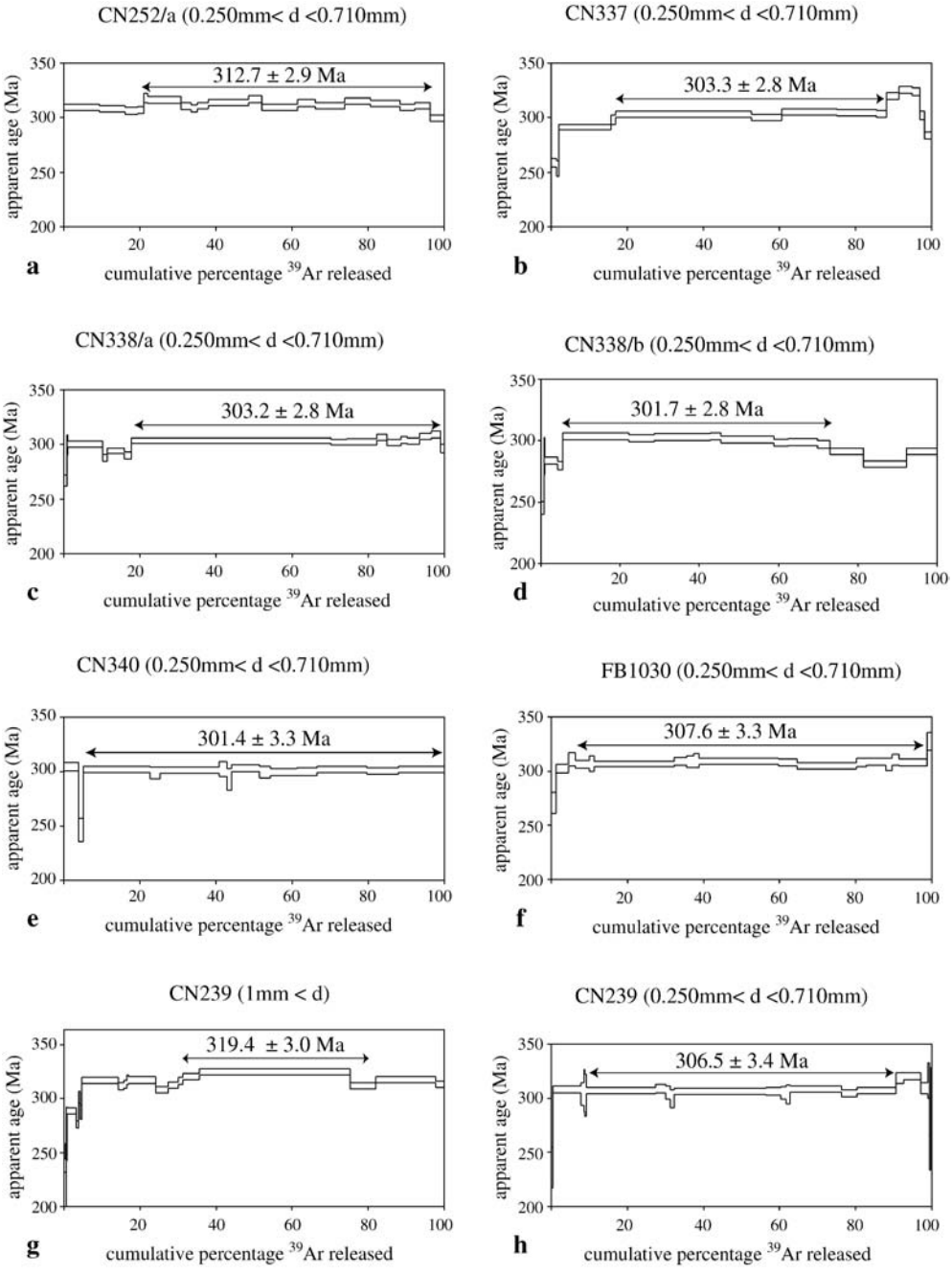

Fig. 8a–h Apparent ages measured by $^{40}Ar/^{39}Ar$ multiple-grain, step-heating technique of muscovite separated from individual boulders. Apparent ages document rapid cooling prior to exposure, erosion and rapid burial. For comparison one sample from the Vallorcine granite was also analysed (Fig. 8f, FB 1030). **a–e** Granitic and pegmatitic boulders; **f** Vallorcine granite; **e–h** gneissic boulder. Description and location of samples in Table 2, Ar-data are available as additional material "Data 1" (see http://dx.doi.org/10.1007/s00531-003-0332-0)

apparent age spectrum in the medium-temperature release steps, giving plateau ages of 302.8±0.9 Ma and 300.6±0.9 Ma (Fig. 9). These values very likely record cooling ages in the source area of the muscovite. The high-temperature argon release steps provided slightly older ages. The total gas ages are 300.9±0.7 (CN 145) and 299.7±0.8 Ma. (CN 146) and are slightly younger because of argon loss in the order of 1–2% (for discussion see below). The non-concordant age spectra appear to represent mixed populations of detrital white mica with small grain sizes and probably slightly different cooling ages. However, apparent ages of samples CN 145 and CN 146 seem also to indicate homogeneous sources of detrital muscovite. The other five samples displayed internally discordant $^{40}Ar/^{39}Ar$ apparent age spectra and are not reported here.

To avoid dating of mixed mica populations, we dated detrital single-grains by $^{40}Ar/^{39}Ar$ total-fusion techniques. Forty-five muscovite grains (0.25–0.71 mm) were separated from samples taken from six different stratigraphic levels (Fig. 4). Ages range between 339.5±4.8 and 279.6±2.6 Ma, with a peak frequency between ca. 302 and ca. 315 Ma (Fig. 10, data available as additional material "Data 2", see http://dx.doi.org/10.1007/s00531-003-0332-0). Some samples (e.g., CN 164; Fig. 11c) display a progressively younging age range (see below).

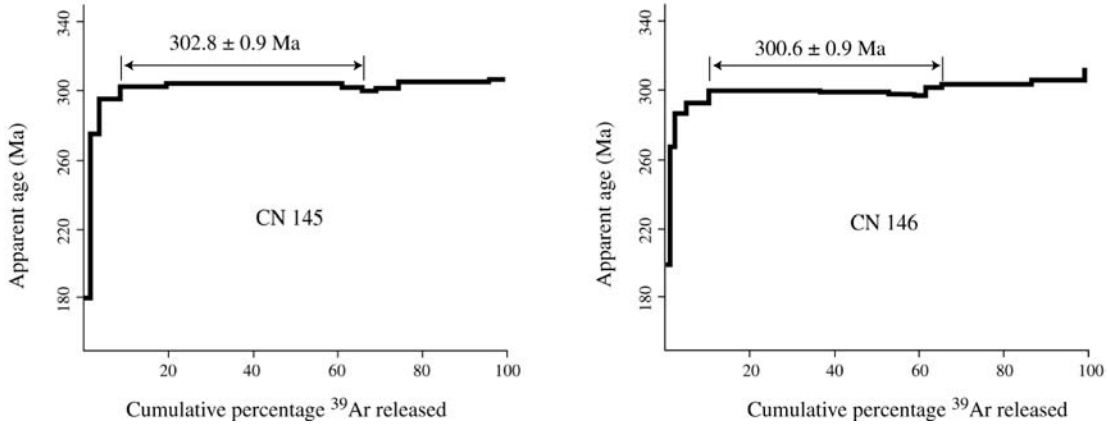

Fig. 9 Detrital muscovite apparent ages measured by $^{40}Ar/^{39}Ar$ multiple-grain, step-heating technique; two sandstones layers (see text for details). Location and stratigraphic position of samples are given in Table 2 and in Fig. 4

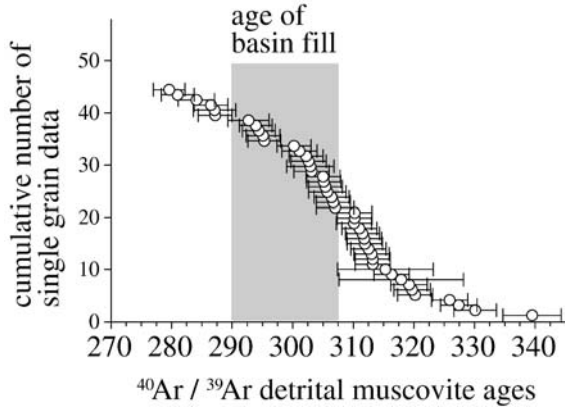

Fig. 10 Entire spectrum of detrital muscovite ages measured by $^{40}Ar/^{39}Ar$ single-grain, total fusion technique, for all the investigated Late Carboniferous clastic sediments. Bar length corresponds to 2σ error; the recorded muscovite ages are plotted from the old to young, clustering between ca. 302 and 315 Ma. Ar data are available as additional material ("Data 2", see http://dx.doi.org/10.1007/s00531-003-0332-0). The *grey vertical bar* refers to the age of the sediments in the Salvan-Dorénaz basin

Other samples indicate distinct populations of muscovite, with older age groups of ca. 340–330 and ca. 320–325 Ma, and distinctly younger ages of ca. 312 and ca. 305 Ma (e.g., CN 116, CN 136; Fig. 11d, f). The older ages are more frequent within upper stratigraphic levels (e.g., CN 116, CN 136).

Some of the ages obtained from $^{40}Ar/^{39}Ar$ total-fusion experiments yielded ages younger than the stratigraphic age of the host sediment. This might be due to minor radiogenic Ar loss of some of the micas after initial cooling. A minor, post-depositional argon loss in the order of one to maximum two percent is similar to that observed in multiple-grain samples CN 145 and CN 146 (Fig. 9; for discussion see below).

Post-depositional argon loss

To evaluate post-depositional argon loss and its younging effects, we additionally measured four bulk-grain samples of such muscovites by incremental heating technique and checked if we could see some disturbances in the Ar-release spectra (Fig. 12a–d; data available as additional material "Data 3", see http://dx.doi.org/10.1007/s00531-003-0332-0). All samples display more or less undisturbed age spectra in the medium- and high-temperature gas release steps. Ages integrated from these steps range between 297.5±4.0 Ma (CN 214; Fig. 12d) and 308.2±3.1 Ma (CN 131; Fig. 12b), which is well in accordance with results obtained on smaller size fractions of other samples (e.g., CN 145, CN 146; Fig. 9), the single-grain analyses, and results from $^{40}Ar/^{39}Ar$ incremental heating experiments on bulk-grain samples from magmatic and metamorphic boulders (see above). However, the first steps of all release spectra display younger ages, ranging between ca. 280 and 220 Ma, which indicates loss of radiogenic Ar components after initial closure of the system. This might serve as an explanation for the obvious discrepancy of detrital micas, which record younger $^{40}Ar/^{39}Ar$ ages than the stratigraphic age of their host sediment (e.g., Copeland and Harrison 1990).

Interpretation and discussion

The continental sediments of the Salvan-Dorénaz basin are texturally and compositionally immature. The abundance of lithic clasts and detrital minerals with low chemical and mechanical stability indicates that they accumulated not far away from their source areas and experienced only limited physical and chemical weathering (e.g., Tucker 1991). The sediment composition documents granitic, volcanic, low- and high-grade metamorphic, and some meta-sedimentary rocks outcropping in the catchment areas. Among these components, significant variations between prevalent magmatic and

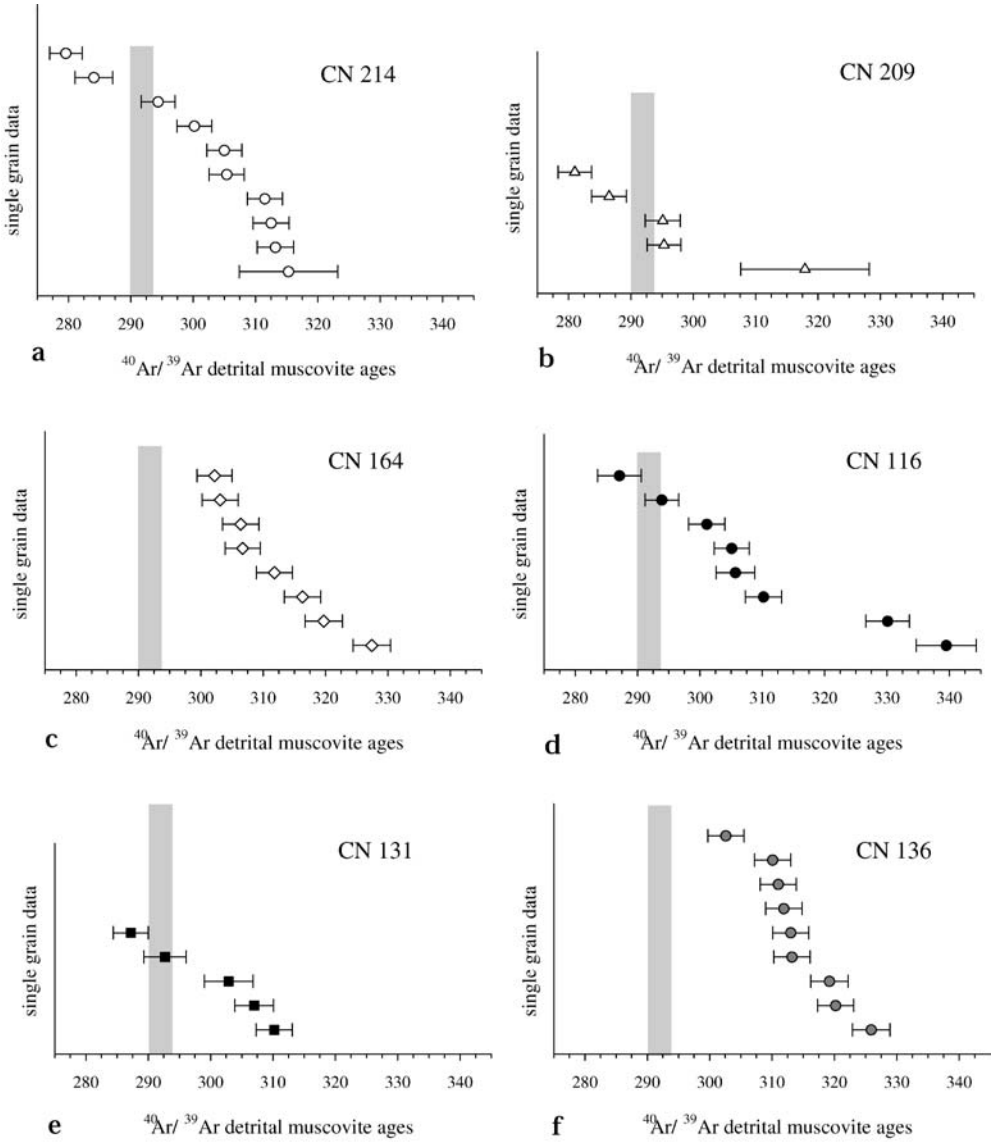

Fig. 11 Detrital muscovite ages, measured by $^{40}Ar/^{39}Ar$ single-grain, total fusion technique, shown from base (**a**) to top (**f**). *Bar length* corresponds to 2σ error. The *grey vertical bar* refers to the age of the uppermost sediments in the Salvan-Dorénaz. Ar data are available as additional material ("Data 2", see http://dx.doi.org/10.1007/s00531-003-0332-0). Location and stratigraphic position are given in Table 2 and Fig. 4

prevalent metamorphic boulders imply temporal lithological changes in the eroded source material. Chemical weathering could have been favoured by humid climatic regimes at that time (e.g., Nesbitt and Young 1982, 1989), possibly induced by high altitude levels reached in the internal parts of the Variscan mountain range (e.g., Becq-Giraudon and van den Driessche 1994). This is also assumed for the Salvan-Dorénaz basin at least during its initial phase of development (Capuzzo and Wetzel 2003).

The coarse boulders within the lower sedimentary unit indicate a nearby source and a steep relief. From the NW, debris flows and braided river systems transported large amounts of clastic materials into the basin (Capuzzo and Wetzel 2003). Granitic boulders have a geochemical signature similar to that of the Vallorcine and Montenvers anatectic granites, which outcrop only a few km away (Fig. 2; Morard 1998; Bussy et al. 2000. Despite alteration of feldspars, the major elements document only short-term exposure at the surface during weathering, transport, and deposition (Fig. 6). The geochronology and composition of the boulders (Fig. 8) imply that their parent rocks were probably emplaced during the intense syntectonic magmatic activity that occurred at different crustal levels during the final stages of the Variscan collision (e.g., Bonin et al. 1993; Brändlein et al. 1994; Schaltegger 1994; Finger et al. 1997; Bussy et al. 2000). Apparent $^{40}Ar/^{39}Ar$ ages of muscovites from these boulders range between 312.7±2.9 and 301.4±3.3 Ma (Fig. 8) and are interpreted to record their rapid isothermal decompression, favoured by dextral transtensional strike-slip regimes (e.g., Schulz and von Raumer 1993; Brändlein et al. 1994). The erosion of Late Carboniferous granites during the latest Westphalian–early Stephanian indicates rapid exhumation leading to the exposure of mid-crustal levels at the surface, as it has been reported, for instance, by Menning et al. (2000). On the other hand, pegmatitic grain size and trace-element concentrations indicate a late-magmatic stage of hydrothermal circula-

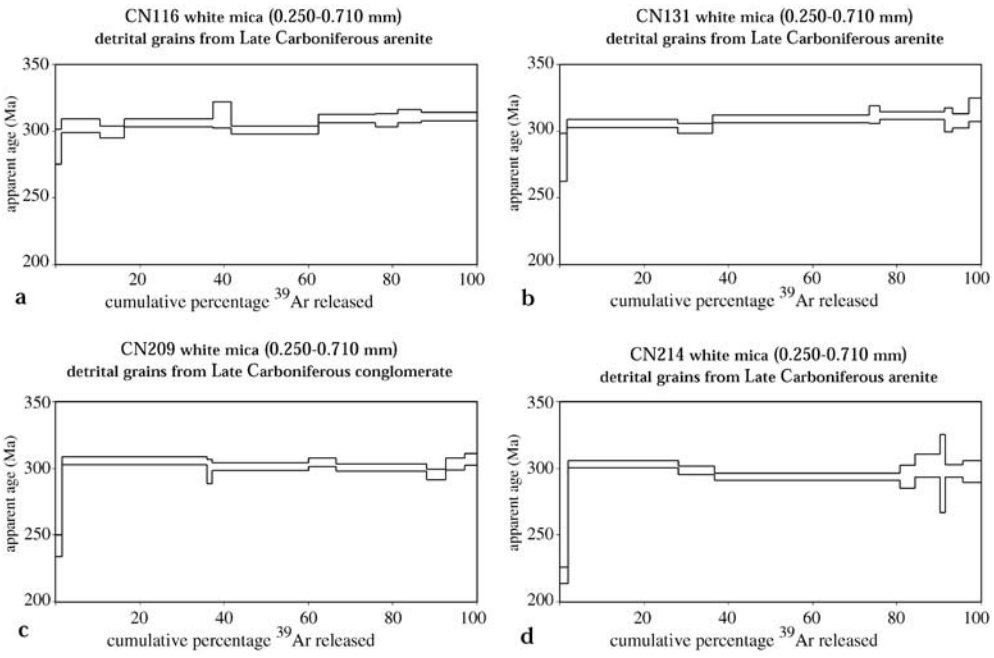

Fig. 12 $^{40}Ar/^{39}Ar$ ages of four samples of detrital white mica measured from multiple (10–15) grains. Ar data are available as additional material ("Data 3", see http://dx.doi.org/10.1007/s00531-003-0332-0). Location and stratigraphic position are shown in Table 2 and Fig. 4

tion, as commonly described in the Late Variscan magmatic activity (e.g., Simon 1990), that has also been recorded by the emplacement of the Vallorcine granite (Brändlein et al. 1994). Source areas of the boulders, therefore, were very probably muscovite±biotite granites in the nearby Aiguilles-Rouges massif (Fig. 2).

The range of $^{40}Ar/^{39}Ar$ ages from ca. 290–339 Ma of detrital muscovite within boulder-hosting sandstone points to erosion of basement units which had different P–T histories (Fig. 11): (1) a unit with early Carboniferous ages between 320 and 340 Ma, and (2) a unit with young ages between ca. 315–302 Ma. This second unit includes the Vallorcine-type granite and country rocks which were thermally overprinted by this type of intrusion. No older ages than ca. 339 Ma have been found. This suggests that the entire catchment area was dominated by Variscan metamorphic and plutonic rocks. We estimate an average of about 1% radiogenic argon loss implying that reported ages are about 1% too young. The measured ages are similar to isotopic ages from different metamorphic and magmatic units in the vicinity of the basin (Fig. 2; Schulz and von Raumer 1993; Dobmeier 1998; von Raumer 1998; Bussy et al. 2000).

We suggest that partial diffusive resetting due to post-depositional very-low-grade metamorphism is the process which can explain the too-young ages. The prime argument for that interpretation is the shape of age spectra which show the diffusive argon loss in low-temperature increments of the experiment. Furthermore, we carefully selected grains without any alteration along their margins and without any inclusions. We exclude therefore the possibility of minor loss of radiogenic Ar components due to weathering and erosion before deposition.

The time interval between initial closure of the Ar isotopic system in the muscovites as indicated by the $^{40}Ar/^{39}Ar$ ages and the time of basin formation was very short (Fig. 10). In fact, after reaching the argon retention temperature of muscovite (T_c>350±50 °C) the parent rocks must have been exhumed to the surface, eroded and transported to their final depositional site within only few million years; detrital muscovite ages cluster between ca. 302 and ca. 315 Ma (Fig. 10). This possibly represents the time of cooling and rapid rock uplift of basement units within the catchment areas of the basin. In addition, the narrow range of the detrital muscovite ages at various stratigraphic levels of the Salvan-Dorénaz basin indicates very fast cooling of the basement being eroded, since older detrital mineral ages are more frequently represented in its upper levels. These results are consistent with the inferred Late Variscan tectonic evolution of the region, where prevalent transtensional strike-slip regimes controlled isothermal decompression of the pre-existing Variscan metamorphic zonation (Schulz and von Raumer 1993; Dobmeier 1998) and concomitant syntectonic intrusions, at shallow crustal levels, of anatectic melts (Brändlein et al. 1994; Morard 1998).

Alternatively, the observed up-section variation in detrital muscovite ages might reflect that the catchment area grew in size with time and increasingly received material having older cooling ages. This scenario is quite likely for the lithologic Units I and III at the base and the top of the basin fill respectively, that display such "aging upward" (Figs. 4, 11; Unit I: CN 164, 209, 214; Unit III: CN 131, 136). During the formation of these units, sediment composition and the depositional style by a braided and a meandering river, respectively, do not document a significant change and hence, may indicate relative stability. In contrast the anastomosed river

deposits of Unit II display very narrow and young age spectra (CN 145, CN 146; Figs. 4, 9) pointing to a homogeneous and restricted source area likely across a major, regional normal fault (e.g., von Eynatten et al. 1999). Just at that time the paleo-drainage direction became reversed and the basin is inferred to have subsided at an increased rate (e.g., Niklaus and Wetzel 1996). Therefore a tectonic rearrangement of the whole basin is inferred and very likely of the catchment areas too.

Due to both the limited stratigraphical resolution of the Salvan-Dorénaz basin and to the possibility of sedimentary mixing between different catchment areas, the measured detrital muscovites ages allow no precise determinations of the exhumation rates in the source areas. Nonetheless, exhumation was rapid, which is in good agreement with average rate of ~1 mm/y calculated for the Late Variscan uplift in the Aiguilles-Rouges massif (Capuzzo and Bussy 2000). Further evidence for the rapid cooling of basement units outcropping in the catchment areas of the basin is provided by muscovite ages of one gneissic boulder from a low stratigraphical level (CN 239; Fig. 8g, h). As often observed in metamorphic rocks, muscovites display radiogenic retention ages dependent, among other factors like cooling rate, matrix minerals and deformational state, on their grain-size, whereby the intensity of the grain-size controlled diffusional Ar loss depends on the cooling rate of the parent rock (Villa 1998; McDougall and Harrison 1999). In this specific case (CN 239; Fig. 8g, h), the age difference between the two grain sizes of mica, 250–710 and >1,000 μm, respectively, seems to indicate cooling with rates of ca. 5 °C/Ma (M. Cosca, Lausanne, personal communication). The white mica extracted from the Vallorcine granite has an apparent age of ca. 307 Ma (FB 1030; Fig. 8f), which is—within the analytical errors—identical to its U/Pb zircon and monazite retention ages (Bussy et al. 2000) and thus documents rapid cooling and confirms shallow crustal emplacement of this Late Carboniferous intrusion (Brändlein et al. 1994). However, the gneiss boulder (sample 239) must originate from an earlier and higher level of the Variscan pluton and is not identical to the Vallorcine granite. This is also shown by the seemingly slow cooling rate inferred from different grain sizes from the same sample.

More insights into the nature and origin of the Salvan-Dorénaz clastic sediments come from the interpretation of the detrital muscovites ages. They all document erosion of young material (Figs. 9, 10, 11), when compared to U/Pb isotopic ages of basin formation (Fig. 2; Capuzzo and Bussy 2000). P–T path of metamorphic basement rocks from the Aiguilles Rouges region suggest a two-stage exhumation (e.g., Dobmeier 1998): a first stage with nearly isothermal decompression from ca. 10 to ca. 6–4 kbar and then concomitant cooling and decompression with a geothermal gradient of 50–60 °C/km. If we assume an elevated thermal gradient of 60 °C/km, a major portion of the upper crust (about 6 km) was removed prior to the formation of the basin, and suggests extremely rapid post-collisional exhumation (>1–2 mm/year). In comparison, detrital muscovite single-ages in Variscan basins of the Eastern Alps (Handler et al. 1997; Mader et al. 2000), in the Moravo-Silesian basin of the Czech Republic (Schneider et al. 2000) and in peripheral molasse basins in the Himalayas (Najman et al. 1997) show a similar pattern with ca. 95% of detrital muscovites eroded from young material. In the Alpine Molasse basin, however, only 20–25% of the white micas cooled through the argon retention temperature during the same orogenic cycle (von Eynatten et al. 1999). This contrasts with material from the Salvan-Dorénaz basin which comprises exclusively young micas formed during the same orogenic cycle. Consequently, this indicates a fundamental difference between the Variscan and Alpine orogens. Therefore, the case of the Late Paleozoic Salvan-Dorénaz basin proves extremely rapid removal of the upper sector of the crust, which appears unusual, especially if compared with the Alpine and Himalaya orogens (Neubauer et al. 2000). For example, in Cenozoic Tibetan basins only "old" detrital material was found, which suggests surface uplift but not much erosion and exhumation (Harrison et al. 1993). Locally, an extremely rapid Pliocene–Quaternary exhumation and present-day denudation of anatectic metamorphic rocks has been observed in the Himalayan syntaxis area (e. g. Zeitler et al. 1993; Treloar et al. 2000) which contributes to young ages of detrital minerals in Neogene-Quaternary basins of the Himalayan area (Copeland and Harrison 1990; Najman et al. 1997) although no collapse occurred and the Himalayan crust is still anomalously thick.

The Variscan orogeny, however, appears to be quite different due to both high exhumation and erosion, possibly as a consequence of humid climatic conditions, which is supported by trace element geochemical evidence for Late Variscan deep weathering. Extensional collapse in combination of high rock uplift and surface and/or tectonic erosion of the Variscan orogen is an appropriate model to explain the presence of exclusively "young" mica ages. Alternatively, a Wernicke-type extension and exhumation of a metamorphic core complex does not seem an appropriate model because these mechanisms always leave an upper, brittle plate behind which would show old, pre-orogenic ages and which is therefore not affected by bulk younging of the upper plate. In all these models, sedimentary basins are limited to the upper, brittle plate.

Conclusions

Different geological processes characterised the Late Paleozoic post-collisional evolution of the European Variscan orogeny and contributed to form and fill several intramontane continental basins. In the investigated area, the post-collisionally thickened crust, which formed during the Variscan orogeny, was thinned to normal extent by rapid exhumation of the basement, syntectonic intrusion of granitic melts, active volcanism of crustal

origin, and basin formation. Tectonic processes coupled with intense erosion produced abundant clastic material that accumulated within the rapidly subsiding Salvan-Dorénaz basin during the Late Carboniferous. In its catchment area predominately granitic, volcanic, and high- and low-grade metamorphic rocks cropped out and document that the Variscan orogenic roots were already exposed and being eroded in the Late Carboniferous. The detrital muscovite ages are similar to the stratigraphic age of their host sediments and, hence indicate rapid cooling and—very probably—exhumation of the basement during basin formation. Since only "young" Variscan material accumulated in the basin, the entire upper crust has been removed prior to its formation. This implies both, exhumation above the Ar retention temperature and removal of at least 6 km of crust, if an elevated thermal gradient of 60 °C/km is assumed in this internal sector of the Variscan orogenic belt. Age determinations and sediment composition document that highly differentiated granites were syntectonically emplaced at shallow crustal levels, rapidly uplifted to the surface and eroded. Their intrusion was favoured by anatectic decompression melts in the hanging wall of crustal-scale transcurrent fracture zones, which guided their subsequent exhumation. Similar fracture zones also controlled the formation of the Salvan-Dorénaz basin, which was probably the surface response to rapid asymmetric subsidence of the footwall. In addition, high heat flow also caused subvolcanic and hydrothermal activities along similar fractured zones.

If compared with other intramontane molasse basins formed during post-collisional extension in modern and ancient orogenic belts, this study underlines the peculiarity of the Variscan post-collisional horst and basin formation; simultaneously acting, rapid exhumation of the orogenic roots and intense erosion—which may be favoured by humid climatic conditions—led to exclusively young ages of detrital material, a case rarely reported yet.

Acknowledgements F. Bussy (Lausanne) helped the first author in the field to select boulders and to classify them, F. Bussy in addition provided a sample from the upper levels of the Vallorcine granite (FB 1030). M. Cosca (Lausanne) contributed numerous and helpful discussions and carried out some of the $^{40}Ar/^{39}Ar$ multiple-grain, step-heating age determinations on detrital muscovites. H. Pfeiffer, J. Lavanchy and H. Hunziker (all at Lausanne) provided support during geochemical analyses and mineral separation. H. Genser, G. Friedl and D. Schneider (Salzburg) assisted when performing some of the $^{40}Ar/^{39}Ar$ analyses. J. von Raumer (Fribourg), Wijbrands (Amsterdam) and—as journal reviewers—A. Henk (Freiburg) and an anonymous colleague provided helpful comments. This research was funded by the Swiss National Science Foundation (grants nos. 21-43103.95 and 20-50484.97 to A. Wetzel). All these contributions are gratefully acknowledged.

Appendix

Detailed description of the analytical methods

Samples were polished from their weathered margins, except the strongly altered sample CN 252/a which was not considered for geochemical analyses. In addition, the same analytical techniques were applied for comparison on sample FB1030, from the upper levels of the "stratified" Vallorcine granite (Fig. 2; Brändlein et al. 1994), while on sample CN 331, from the lower levels of the same granitic intrusion, only XRF whole rock trace elements analyses were performed. A short description and the location of this second set of samples are reported in Table 2.

After gently crushing and sieving the samples, muscovites were concentrated from a grain size between 0.25–0.71 mm by standard separation techniques in the mineral separation laboratory at the University of Lausanne, Switzerland. The sieved samples were milled using an agate mill with ethnol as diluent, sieved again to remove the suspended fraction, and then dried at 50 °C. The mineral concentrates were then sent to the University of Salzburg and handpicked under a binocular microscope into Al-foil capsules, sealed in quartz vials, and irradiated for 8 h in the central position of the ASTRA reactor at the Austrian Research Center in Seibersdorf, Austria. Flux within the reactor was 1.1×10^{14} n/cm^{2}s, correction factors for interfering isotopes have been reported by Frank et al. (1996) and are: $^{36}Ar/^{37}Ar_{(Ca)}=0.0003$, $^{39}Ar/^{37}Ar_{(Ca)}=0.00065$, and $^{40}Ar/^{39}Ar_{(K)}=0.03$. Variation in the flux of neutrons were monitored with B4 M white mica standard (Flisch 1982) for which a $^{40}Ar/^{39}Ar$ plateau age of 18.555±0.4 Ma has been reported (Burghele 1987). The $^{40}Ar/^{39}Ar$ isotopic analyses were carried out at the Institute for Geology and Paleontology at the University Salzburg using a UHV Ar-extraction line equipped with a combined MERCHANTEK™ UV/IR laser ablation facility, and a VG-ISOTECH™ NG3600 Mass Spectrometer. Single-grain total-fusion (data available as additional material "Data 1") and bulk-grain stepwise-heating (data available as additional material "Data 2"; see http://dx.doi.org/10.1007/s00531-003-0332-0), analyses of muscovites were performed using a 25 W CO_2-IR laser operating in Tem_{00} mode at wavelengths between 10.57–10.63 μm. The laser was defocused to a spot size of ca. 1.0 mm and controlled by a PC. On a computer screen the position of the laser on the sample was monitored through a double-vacuum window on the sample chamber via a video camera in the optical axis of the laser beam. Gas clean up was performed using one hot and one cold Zr-Al SAES getter. Gas admittance and pumping of the mass spectrometer and the Ar-extraction line were computer controlled using pneumatic valves. The VG3600 is an 18-cm radius 60° extended geometry instrument, equipped with a Nier-type Bright Source operated at 4.5 kV. Measurements were performed in static mode on an axial electron multiplier and peak-jumping and stability of the magnet was controlled by a Hall-probe. For each increment the intensities of ^{36}Ar, ^{37}Ar, ^{38}Ar, ^{39}Ar, and ^{40}Ar were measured, the baseline readings on mass 33.5 were automatically subtracted. Intensities of the peaks were back-extrapolated over 16 measured intensities to the time of gas admittance either by a straight line or a curved fit. Intensities were corrected for system blanks, background, post-irradiation decay of ^{37}Ar, and interfering isotopes.

References

Arthaud F, Matte PH (1977) Late Paleozoic strike-slip faulting in Southern Europe and Northern Africa. Geol Soc Am Bull 88:1305–1320

Badertscher N, Burkhard M (1998) Inversion alpine du graben Permo-Carbonifère de Salvan-Dorénaz et sa relation avec le chavauchement de la Nappe de Morcles sus-jacente. Eclogae Geol Helvetiae 91:359–373

Becq-Giraudon JF, van den Driessche J (1994). Dépots periglaciaires dans le Stéphano-Autunien du Massif Central: témoin de l'efondrement gravitaire d'un haut plateau hercynien. C R Acad Sci Paris Sér II, 318:675–682

Bhatia MR, Crook KAW (1986) Trace elements characteristics of greywackes and tectonic setting discrimination of sedimentary basins. Contrib Mineral Petrol 92:181–193

Blair TC, Bilodeau WL (1988) Development of tectonic cyclothems in rift, pull-apart, and foreland basins: Sedimentary response to episodic tectonism. Geology 16:517–520

Bonin B, Brändlein P, Bussy F, Desmons J, Eggenberger U, Finger F, Graf K, Marro C, Mercolli I., Oberhänsli R, Ploquin A, von Quadt A, von Raumer J, Schaltegger U, Steyrer H, Visonà D, Vivier G (1993) Late Variscan magmatic evolution of the Alpine basement. In: von Raumer J, Neubauer F (eds) Pre-Mesozoic geology in the Alps. Springer, Berlin Heidelberg New York, pp 171–201

Brändlein P (1991) Petrographische und geochemische Charakteristika des Vallorcine-Granits, Aiguilles Rouges Massiv (Westalpen, Schweiz). PhD Thesis, University of Fribourg

Brändlein P, Nollau G, Sharp Z, von Raumer J (1994) Petrography and geochemistry of the Vallorcine granite (Aiguilles-Rouges massif, Western Alps). Schweiz Mineral Petrogr Mitt 74:227–243

Burghele A (1987) Propagation of error and choice of standard in the 40Ar-39Ar technique. Chem Geol 66, 17-19

Bussy F, Hernandez J (1997) Short-lived bimodal magmatism at 307 Ma in the Mont-Blanc/Aiguilles-Rouges area: a combination of decompression melting, basaltic underplating and crustal fracturing. 3rd Workshop on Alpine Geological Studies, Oròpa-Biella. Quaderni di Geodinamica Alpina e Quaternaria 4, p 22

Bussy F, Delitroz D, Fellay R, Hernandez J (1997) The Pormenaz monzonite (Aiguilles-Rouges, Western Alps): an additional evidence for a 330 Ma-old magnesio-potassic magmatic suite in the Variscan Alps. Schweiz Mineral Petrogr Mitt 78:193–194

Bussy F, Hernandez J, von Raumer J (2000) Bimodal magmatism as a consequence of the post-collisional readjustment of the thickened Variscan continental lithosphere (Aiguilles-Rouges and Mont-Blanc massifs, Western Alps). Trans R Soc Edinb (in press)

Capuzzo N, Bussy F (2000) High-precision dating and origin of synsedimentary volcanism in the Late Carboniferous Salvan-Dorénaz basin (Aiguilles-Rouges Massif, Western Alps). Schweiz Mineral Petrogr Mitt 80:147–167

Capuzzo N, Wetzel A (2003) Facies and basin architecture of the Late Carboniferous Salvan-Dorénaz continental basin (Aiguilles-Rouges massif, western Alps). Sedimentology (in press)

Cassinis G, Neri C (1990) Collio and Tregiovio Permian continental basins (Southern Alps, Italy): a general comparison. Atti Ticinese Sci Terra 33:11–15

Clarke DB (1992) Granitoid Rocks. Topics in the earth sciences 7. Chapman and Hall, London

Copeland P, Harrison TM (1990) Episodic rapid uplift in the Himalya revealed by $^{40}Ar/^{39}Ar$ analysis of detrital K-feldspar and muscovite, Bengal Fan. Geology 18:354–357

Cortesogno L, Cassinis G, Dallagiovanna G, Gaggero L, Oggiano G, Ronchi A, Seno S, Vanossi M (1998) The Variscan post-collisional volcanism in Late Carboniferous-Permian sequences of Ligurian Alps, Southern Alps and Sardinia (Italy): a synthesis. Lithos 45:305–328

Dallmeyer RD, Takasu A (1992) $^{40}Ar/^{39}Ar$ ages of detrital muscovite and whole-rock slate/phyllite, Narragansett Basin, RI-MA, USA: implications for rejuvenation during very low-grade metamorphism. Contrib Mineral Petrol 110:515–527

Demathieu G, Weidmann M (1982) Les emprintes de pas de reptiles dans le Trias du Vieux Emosson (Finhaut, Valais, Suisse). Eclogae Geol Helvetiae 75:721–757

Dickinson WR (1974) Plate tectonics and sedimentation. In: Dickinson WR (ed) Tectonics and Sedimentation. Soc Econ Paleontol Mineral Spec Publ 22:1-27

Dobmeier C (1998) Variscan P-T deformation paths from the south-western Aiguilles Rouges massif (External massif, western Alps) and their implication for its tectonic evolution. Geol Rundsch 87:107–123

Dobmeier C, von Raumer JF (1995) Significance of latest-Variscan and Alpine deformation for the evolution of Montagne de Pormenaz (south-western Aiguilles-Rouges massif, Western Alps). Eclogae Geol Helvetiae 88:267–279

El Bouseily AM, El Sokkary AA (1975) The relation between Rb, Ba and Sr in granitic rocks. Chem Geol 16:207–219

Finger F, Roberts MP, Haunschmid B, Schermaier A, Steyrer HP (1997) Variscan granitoids of Central Europe: their typology, potential sources and tectonothermal relations. Mineral Petrol 61: 67–96

Flisch M (1982) Potassium-argon analysis. In: Odin GS (ed) Numerical dating in stratigraphy. Wiley, Chichester, pp 151–158

Frank E, Stettler A (1979) K-Ar and $^{40}Ar/^{39}Ar$ systematics of white mica from the alpine metamorphic profile in the Swiss Alps. Schweiz Mineral Petrogr Mitt 59:375–394

Frank E, Lelkes-Felvári G, Dunkl I (1996) K-Ar and $^{40}Ar/^{39}Ar$ systematics of white mica from the alpine metamorphic profile in the Swiss Alps. Schweiz Mineral Petrogr Mitt 59:375–394

Franke W (1989) Tectonostratigraphic units in the Variscan belt of central Europe. Geol Soc Am Spec Pap 230:67–90

Franke W (1992) Phanerozoic structures and events in central Europe. In: Blundell D, Freeman R, Mueller S (eds) A Continent revealed: the European geotraverse. Cambridge University Press, New York, pp 164–180

Franks GD (1968) A study of Upper Paleozoic sediments and volcanics in the northern part of the eastern Aar Massif. Eclogae Geol Helvetiae 61:49–140

Frey M, Desmons J, Neubauer F (1999) Metamorphic Map of the Alps: Schweiz Mineral Petrogr Mitt 79:1–230

Handler R, Dallmeyer RD, Neubauer F (1997) $^{40}Ar/^{39}Ar$ ages of detrital white mica from Upper Austroalpine units in the Eastern Alps, Austria: Evidence for Cadomian and contrasting Variscan sources. Geol Rundsch 86:69–80

Harrison TM, Copeland P, Hall SA, Quade J, Burner S, Ojha TP, Kidd, WSF (1993) Isotopic preservation of Himalayan/Tibetan uplift, denudation and climatic histories of two molasse deposits. J Geol 101:157–175

Henk A (1999) Did the Variscides collapse or were they torn apart?: a quantitative evaluation of the driving forces for post-convergent extension in central Europe. Tectonics 18:774–792

Ingersoll RV (1988) Tectonics of sedimentary basins. Geol Soc Am Bull, 100:1704–1719

Jongmans WJ (1960) Die Karbonflora der Schweiz. Beiträge zur geologischen Karte der Schweiz Neue Folge 108: Schweizerische Geologische Kommission, Bern

Kubler B, Pittion JL, Heroux Y, Charollais J, Weidmann M (1979) Sur le pouvoir réflecteur de la vitrine dans quelques roches du Jura, de la Molasse et des Mappes préalpines, helvétiques et penniques (suiss occidentale et Haute-Savoie). Eclogae Geol Helvetiae 72:347–373

Lox A, Belliére J (1993) Le Silésien (Carbonifére Supérieur) de Pormenaz (Massif des Aiguilles-Rouges): litologie et tectonique. Eclogae Geol Helvetiae 86:769–783

Mader D, Neubauer F, Handler R (2000) Palaeozoic sandstones in the Carnic Alps (Austria): geodynamic setting by geochemistry, detrital mode and $^{40}Ar/^{39}Ar$ dating. Mitt Ges Geol Bergbaustudenten Österr 43:89–90

McDougall I, Harrison TM (1999) Geochronology and thermochronology by the $^{40}Ar/^{39}Ar$ method, 2nd edn. Oxford monographs on geology and geophysics 9. Oxford University Press, Oxford

Ménard G, Molnar P (1988) Collapse of a Hercynian Tibetan Plateau into a late Palaezoic European Basin and Range province. Nature 334:235–237

Menning M, Weyer D, Drozdzewski G, van Ameron HWJ, Wendt I (2000) A Carbonifreous time scale 2000: discussion and use of geological parametres as time indicators from central and western Europe. Geol Jahrb, Reihe A 156: 3–44

Morard A (1998) Pétrographie et cartographie du socle du massif du Mont Blanc dans la région de la Montagne de Lognan (Argentière, France). Diploma Thesis Lausanne

Najman YMR, Pringle MS, Johnson MRW, Robertson, AHF, Wijbrans JR (1997) Laser $^{40}Ar/^{39}Ar$ dating of single detrital muscovite grains from early foreland-basin sedimentary de-

posits in India: Implications for Early Himalayan evolution. Geology 25:435–438
Nesbitt HW, Young GM (1982) Early Proterozoic climates and plate motions inferred from major element chemistry of lutites. Nature 299: 715–717
Nesbitt HW, Young GM (1984) Prediction of some weathering trends of plutonic and volcanic rocks based upon thermodynamic and kinetic considerations. Geochim Cosmochim Acta 48:1523–1534
Nesbitt HW, Young GM (1989) Formation and diagenesis of weathering profiles. J Geol 97:129–147
Nesbitt HW, Fedo CM, Young GM (1997) Quartz and feldspar stability, steady and non-steady state weathering and petrogenesis of siliciclastic sands and muds. J Geol 105:173–191
Neubauer F, Handler R (2000) Variscan orogeny in the Eastern Alps and Bohemian Massif: how do these units correlate? In: Neubauer F, Höck V (eds) Aspects of geology in Austria. Mitt Österr Geol Ges 92:35–59
Neubauer F, Schneider D, Mader D, Handler R (2000) Crustal rejuvenation: Constraints from $^{40}Ar/^{39}Ar$ ages of detrital mica from flysch and molasse basins. 31st International Geological Congress
Niklaus P-A, Wetzel A (1996) Faziesanalyse und Ablagerungsmilieu der fluviatilen Sedimentfüllung des Karbontroges von Salvan-Dorénaz. Eclogae Geol Helvetiae 89:427–437
Pettijohn FJ, Potter PE, Silver R (1987) Sand and Sandstones. Springer, Berlin Heidelberg New York
Pilloud C (1991) Structure de déformation alpines dans le synclinal de Permo-Carbonifere de Salvan-Dorénaz, (massif des Aiguilles Rouges, Valais). Memoirs de Géologie, Lausanne 9
Reuter A, Dallmeyer RD (1989) K-Ar and $^{40}Ar/^{39}Ar$ dating of cleavage formed during very low grade metamorphism: a review. In: Daly JS, Cliff RA, Yardley, BWD (eds) Evolution of metamorphic belts. Geol Soc London Spec Publ 43:161–172
Rollinson H (1993) Using geochemical data: evaluation, presentation, interpretation. Longman, London
Schäfer A, Korsch, RJ (1998) Formation and sediment fill of the Saar-Nahe Basin (Permo-Carboniferous, Germany). Z Dtsch Geol Ges 149:233–69
Schaltegger U (1994) Unravelling the pre-Mesozoic history of Aar and Gotthard massifs (Central Alps) by isotopic dating—a review. Schweiz Mineral Petrogr Mitt 74:41–51
Schaltegger U (1997) Magma pulses in the central Variscan belt: episodic melt generation and emplacement during lithospheric thinning. Terra Nova 9:242–245
Schaltegger U, Corfu F (1995) Late Variscan "basin and range" magmatism and tectonics in the central Alps: evidence from U-Pb geochronology. Geodinamica Acta 8:82–98
Schneider D, Handler R, Tomek C, Kalvoda J, Neubauer F (2000) $^{40}Ar/^{39}Ar$ dating of detrital mica from the Moravo-Silesian basin, Czech Republic. Mitt Ges Geol Bergbaustudenten Österr 43:122–123
Schulz B, von Raumer J (1993) Syndeformational uplift of Variscan high-pressure rocks (Col de Bérard, Aiguilles Rouges Massif, Western Alps). Z Dtsch Geol Ges 144:104–120
Simon K (1990) Hydrothermal alteration of Variscan granites, southern Schwarzwald, Federal Republic of Germany. Contrib Mineral Petrol 105:177–196
Stampfli G (1996) The Intra-Alpine terrain: a Paleotethyan remnant in the Alpine Variscides. Eclogae Geol Helvetiae 89:13–42
Stampfli GM, Mosar J, De Bono A, Vavassis IN (1998) Late Paleozoic, Early Mesozoic plate tectonics of the Western Tethys. 8th International Congress of the Geological Society of Greece, Patras, pp 113–120
Steiger RH, Jäger E (1977) Subcommision on geochronology: convention on the use of decay constants in geo- and cosmochronology. Earth Planet Sci Lett 36:359–362
Stollhofen H, Stanistreet GI (1994) Interaction between bimodal volcanism, fluvial sedimentation and basin development in the Permo-Carboniferous Saar-Nahe Basin (south-west Germany). Basin Res 6:245–267
Sublet P (1962) Etude géologique du synclinal Carbonifére de Collonges-Dorénaz (Valais). Eclogae Geol Helvetiae 55:23–76
Tait JA, Bachdadse V, Franke W, Soffel, HC (1997) Geodynamic evolution of the European Variscan fold belt: paleomagnetic and geological constraints. Geol Rundsch 86:585–598
Treloar PJ, Rex D, Guise P, Wheeler J, Hurford A, Carter A (2000) Geochronologic constraints on the evolution of the Nanga Parbat syntaxis, Pakistan Himalaya. In: Khan A, Searle M, Treloar P (eds) Tectonics of the Nanga Parbat syntaxis and western Himalaya. Geol Soc London Spec Publ 170:137–162
Tucker ME (1991) Sedimentary petrology. Blackwell, London
Villa I (1998) Isotopic closure. Terra Nova 10:42–47
Visser JNJ, Young GM (1990) Major element geochemistry and paleoclimatology of the Permo-Carboniferous glacigene Dwyka Formation and post-Glacial mudrocks in southern Africa. Palaeogeogr Palaeoclimatol Palaeoecol 81:49–57
von Eynatten H, Schlunegger F, Gaupp R, Wijbrans JR (1999) Exhumation of the central Alps: evidence from laser probe dating of detrital white micas from the Swiss Molasse Basin. Terra Nova 11:284–289
von Raumer JF (1971) Das Mont-Blanc-Massiv—Altkristallin im Bereich schwacher alpiner Metamorphose. Schweiz Mineral Petrogr Mitt 51:193–225
von Raumer J (1998) The Palaezoic evolution in the Alps: from Gondwana to Pangea. Geol Rundsch 87:407–435
von Raumer J, Abrecht J, Bussy F, Lombardo B, Ménot R-P, Schaltegger U (1999) The Palaeozoic metamorphic evolution of the Alpine External Massifs. Schweiz Mineral Petrogr Mitt 79:5-22
Weil M (1999) Die Geologie der Montagne Fully im Bereich des Lac de Fully (Wallis, Westschweiz). Diplom Thesis, University of Freiburg
Zeh A, Cosca MA, Brätz H, Okrusch M (2000) Simultaneous horst-basin formation and magmatism during Late Variscan transtension: evidence from $^{40}Ar/^{39}Ar$ and $^{207}Pb/^{206}Pb$ geochronology in the Ruhla Crystalline Complex. Int J Earth Sci 89:52–71
Zeitler PK, Chamberlain CP, Smith, HA (1993) Synchronous anatexis, metamorphism, and rapid denudation at Nanga Parbat (Pakistan Himalaya). Geology 21:347–350
Ziegler, PA (1989) Evolution of Laurussia—a study in Late Palaeozoic Plate Tectonics. Kluwer, Dordrecht
Ziegler PA (1990) Geological Atlas of western and central Europe, 2nd edn. Shell Internationale Petroleum Maatschappij BV, The Hague
Ziegler PA (1993) Late Palaeozoic–Early Mesozoic plate reorganization: Evolution and demise of the Variscan fold belt. In: von Raumer JF, Neubauer F (eds) Pre-Mesozoic geology of the Alps. Springer, Berlin Heidelberg New York, London, pp 203–216
Ziegler PA, Stampfli GM (2001) Late Palaeozoic–Early Mesozoic plate boundary reorganization: collapse of the Variscan orogen and opening of Neotethys. In: Cassinis G (ed) Permian continental deposits of Europe and other areas. Regional reports and correlations. Ann Mus Civ Sc Nat Brescia, Monogr "Natura Bresciana" 25:17–34